

Dalton Transactions

Accepted Manuscript



This is an *Accepted Manuscript*, which has been through the Royal Society of Chemistry peer review process and has been accepted for publication.

Accepted Manuscripts are published online shortly after acceptance, before technical editing, formatting and proof reading. Using this free service, authors can make their results available to the community, in citable form, before we publish the edited article. We will replace this *Accepted Manuscript* with the edited and formatted *Advance Article* as soon as it is available.

You can find more information about *Accepted Manuscripts* in the [Information for Authors](#).

Please note that technical editing may introduce minor changes to the text and/or graphics, which may alter content. The journal's standard [Terms & Conditions](#) and the [Ethical guidelines](#) still apply. In no event shall the Royal Society of Chemistry be held responsible for any errors or omissions in this *Accepted Manuscript* or any consequences arising from the use of any information it contains.



Journal Name

ARTICLE

The conjugates of ferrocene-1,1'-diamine and amino acids. A novel synthetic approach and conformational analysis

Monika Kovačević,^a Ivan Kodrin,^{*b} Mario Cetina,^c Ivana Kmetič,^a Teuta Murati,^a Mojca Čakić Semenčić,^a Sunčica Roca^d and Lidija Barišić^{*a}

Received 00th January 20xx,
Accepted 00th January 20xx

DOI: 10.1039/x0xx00000x

www.rsc.org/

A novel synthetic approach toward a poorly explored bioorganometallics consisted of ferrocene-1,1'-diamine bearing structurally and chirally diverse amino acid sequences is reported. Until now, the ferrocene-1,1'-diamine was suitable to accommodate only identical amino acid sequences at its *N*-termini, leading to the symmetrically disubstituted homochiral products stabilized through 14-membered intramolecular hydrogen-bonded ring as is seen in antiparallel β -sheet peptides. The key step of the novel synthetic pathway is transformation of Ac-Ala-NH-Fn-COOH (**5**) (Fn = 1,1'-ferrocenylene) to orthogonally protected Ac-Ala-NH-Fn-NHBoc (**7**). The spectroscopic analysis (IR, NMR, CD) of the novel compounds, corroborated with DFT studies, suggests the interesting feature of the ferrocene-1,1'-diamine scaffold. The same hydrogen-bonding pattern, *i.e.* 14-membered hydrogen-bonded ring, was determined both in solution and in the solid state, thus making them promising, yet simple scaffolds capable to mimic β -sheet peptides. *In vitro* screening of potential anticancer activity in Hep G2 human liver carcinoma cells and Hs 578T human breast cancer cells revealed a cytotoxic pattern for novel compounds (150-500 μ M) with significantly decreased cell proliferation.

Introduction

Reverse turns are structural features of proteins and peptides at which a polypeptide chain changes its direction enabling a protein to fold back on itself.¹ Besides the role in protein folding,² turns are involved in molecular recognition processes mediated through interactions of side chains within the turns with various receptor domains.^{1,3} Depending on a hydrogen-bonded ring size (7-, 10- or 13-membered), turns are classified as γ -, β - and α -turns, respectively. The β -turns are the most abundant motif in folded proteins.¹ As an essential components of β -hairpins (the fundamental elements of anti-parallel β -sheets), the β -turns are considered as a nucleators or initiation sites that bring the two peptide strands in close proximity, enabling their interactions through hydrogen bonding.⁴ While a proper β -sheet-mediated protein folding is essential for normal biological function, the protein misfolding or folding in a fatal way might cause extracellular or intracellular aggregates formation involved in triggering diseases.⁵ The small model compounds containing molecular templates capable of inducing

β -sheet structures in attached peptide strands have been very useful in studies of β -sheet folding and interactions.⁶ Very recently, Sanjayan *et al.* gave an overview of the selected synthetic turn mimetics and hairpin nucleators reported during the past 30 years, with an emphasis on their great potential in the fields of peptide based drugs and organic asymmetric synthesis.⁷

On the basis of the previous results, 1,*n*-disubstituted ferrocenes are established as molecular templates for the design of turns and β -sheet-like structures as the almost free rotating cyclopentadiene (Cp) rings are separated by about 3.3 Å which is ideal for interstrand hydrogen bonding in their conjugates comprised of natural amino acids or peptides.⁸ If peptide groups directly attached to ferrocene template are taken into account, then three major classes of bioconjugates **1-3** derived from ferrocene-1,1'-dicarboxylic acid [(Fcd), **1**]⁹, 1'-amino-ferrocene-1-carboxylic acid [(Fca), **2**]¹⁰ and ferrocene-1,1'-diamine [(Fcda), **3**]¹¹ need to be considered (Fig. 1). The ferrocene scaffolds Fcd, Fca and Fcda were recognized as turn-inducers in peptides **1-3** owing to the presence of 10- (**1**), 12- (**2**) and 14-membered (**3**) intramolecularly hydrogen bonded (IHB) rings.

Ferrocenes **3** derived from Fcda are only poorly examined. While peptides **1** and **2** have been the subject of numerous papers, only one paper describing the two symmetrically disubstituted homochiral peptides Fn-(NH-AA-Boc)₂ (**3a**,

^a Department of Chemistry and Biochemistry, Faculty of Food Technology and Biotechnology, University of Zagreb, Pierottijeva 6, Zagreb, Croatia. E-mail: lidija.baristic@pbf.hr

^b Department of Chemistry, Faculty of Science, University of Zagreb, Horvatovac 102a, Zagreb, Croatia. E-mail: ikodrin@chem.pmf.hr

^c Department of Applied Chemistry, Faculty of Textile Technology, University of Zagreb, Prilaz baruna Filipovića 28a, Zagreb, Croatia.

^d NMR Centre, Ruđer Bošković Institute, Bijenička cesta 54, Zagreb, Croatia.

Electronic Supplementary Information (ESI) available: [details of any supplementary information available should be included here]. See DOI: 10.1039/x0xx00000x

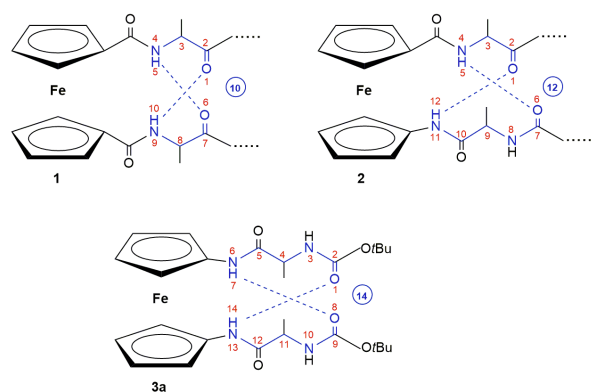
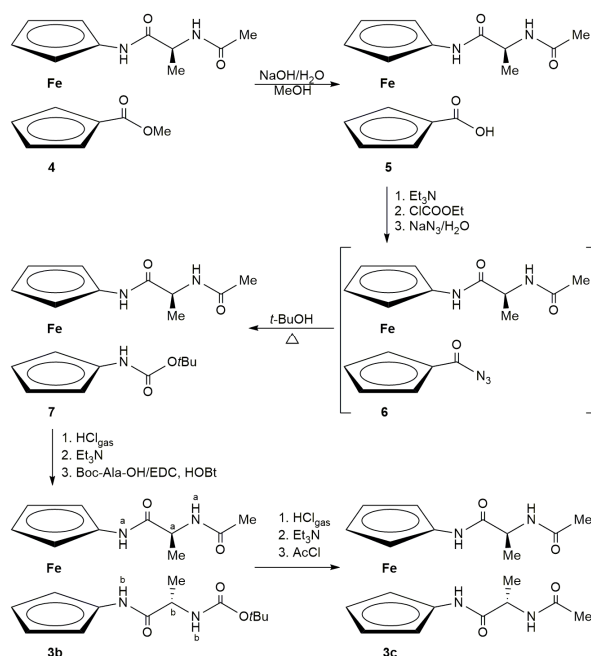


Figure 1. The ferrocene-containing peptides 1-3.

AA = L- or D-Ala), derived from $\text{Fn}(\text{NH}(\text{Boc})_2)_2$, was reported by Kraatz *et al.*¹¹ In that research, the ferrocene-1,1'-diamine acted as turn-inducing scaffold, facilitating the formation of 14-membered rings between attached symmetrical peptide chains, very similar to those found in antiparallel β -sheet peptides. This feature was not yet observed in derivatives **1** and **2**. It seems that the ferrocene-1,1'-diamine framework is a desired structural requirement if we want to further explore and utilize the connection between ferrocene-based peptides and the turn-inducing scaffolds capable to mimic the natural structure of antiparallel β -sheet. Therefore, we were prompted to find a new synthetic route to conjugates **3**, but now bearing structurally and chirally diverse amino acid sequences at its *N*-termini to check their affinity to preserve the conformational motif comprised of two ferrocene-involved 10-membered IHB rings. Acting as a simple model made of only two amino acids, **3** could be considered as the lowest homologues and a step toward the more complex structures mimicking anti-parallel β -sheets.

In this paper, a new synthetic approach toward unsymmetrically substituted ferrocenes **3** is discussed and employed for the first time to prepare orthogonally protected Ac-Ala-NH-Fn-NH-Ala-Boc (**3b**). In addition, acetamide-protected Fn-(NH-Ala-Ac)₂ (**3c**) is also reported (Scheme 1). Since previously described Boc-protected **3a** was stabilized through the two simultaneous interchain $\text{NH}_{\text{Fn}} \cdots \text{OC}_{\text{Boc}}$ IHBs engaged in 14-membered ring, our goal was to explore whether the replacement of one or both Boc-groups of **3a** with sterically less demanding Ac-groups in **3b** and **3c** will affect the IHB pattern. Thereat, the nonpolar and nonbulky side chain of Ala was not expected to interfere with hydrogen bonding.¹² A detailed conformational analysis using spectroscopic (IR, NMR, CD) and computational study together with X-ray crystal structure analysis was performed to clarify IHB patterns of the synthesized compounds and to discuss (di)similarities in solution and in the solid state. Today, a lot of endeavour is directed at creating novel metal-based therapeutics with less negative medical and physical side-effects. Therefore, the newly synthesized derivatives were subjected to biological evaluation to test their potential anticancer activity.



Scheme 1. The synthesis of the goal compounds **3b** and **3c**. (The atom numeration of **3b** used for NMR analysis).

Experimental

Materials and general methods

All reactions were carried out under argon atmosphere. The CH_2Cl_2 used for synthesis and FTIR was dried (P_2O_5), distilled over CaH_2 , and stored over molecular sieves (4 Å). *t*-BuOH was dried with CaH_2 , distilled and stored over molecular sieves (4 Å). EDC (Acros Organics), HOBT (Aldrich), acetyl chloride (Aldrich) and alanine (Acros Organics) were used as received. The syntheses of Ac-Ala-Fca-OMe (**4**) had been previously described.¹³ The *N*-terminus of alanine was protected by using sodium hydroxide, aqueous dioxane and di-*tert*-butyldicarbonate to give Boc-Ala-OH. Products were purified by preparative thin layer chromatography on silica gel (Fluka Silika gel on TLC Al foils, silica gel matrix, with fluorescent indicator 254 nm, layer thickness 0.2 mm). Infrared spectra were recorded as CH_2Cl_2 solutions between NaCl windows by using a Bomem MB 100 mid FTIR spectrometer. (s) = strong, (m) = medium, (w) = weak. All ^1H NMR spectra measured at 600.133 MHz and 300 MHz and ^{13}C NMR spectra measured at 150.917 MHz and 75.432 MHz using Bruker Avance spectrometer, were referenced to the residual solvent peak (CDCl_3 , ^1H : 7.26 ppm, ^{13}C : 77.16 ppm). In the case of the $\text{CDCl}_3/d_6\text{-DMSO}$ mixture, the calibration was done using Me_4Si . Double resonance experiments (COSY, NOESY and HMBC) were performed in order to assist in signal assignment. (s) = singlet, (d) = doublet, (q) = quartet, (dq) = doublet of quartet, (m) = multiplet. Unless otherwise noted, all spectra were recorded at 298 K. CD spectra were recorded using a Jasco-810 spectropolarimeter in CH_2Cl_2 and $\text{CH}_2\text{Cl}_2/\text{DMSO}$ mixture. Molar ellipticity coefficients, $[\theta]$, are in degrees,

concentration, c , is given in mol L⁻¹, and path length, l , is given in cm, to give units for $[\theta]$ of deg cm² dmol⁻¹. NMR titrations were performed by adding of 10 μ L portions of the d_6 -DMSO in a NMR-tubes containing solutions of the examined peptides **3b** and **3c** in CDCl₃ ($c = 2.5 \times 10^{-2}$ M). The spectra were recorded after each addition and d_6 -DMSO was added until no further changes in the chemical shifts of the NHs were observed. CD titrations were performed in a similar manner by stepwise addition of DMSO into cuvettes containing solutions of the examined peptides **3b** and **3c** in CH₂Cl₂ ($c = 5 \times 10^{-3}$ M). Mass spectra were measured on a HPLC-MS system coupled with triple-quadrupole mass spectrometer, operating in a positive ESI mode. High-resolution mass spectra were acquired using 4800 MALDI TOF/TOF-MS Analyzer.

Synthesis of Ac-Ala-NH-Fn-COOH (5)

A solution of **4** (500 mg, 1.34 mmol) in MeOH (3 ml) was heated at 80 °C in the presence of NaOH (53.7 mg, 1.34 mmol) and H₂O (0.2 ml). After 1 h, the reaction mixture was evaporated to dryness. The residue was dissolved in 5% NaHCO₃ and extracted with CH₂Cl₂ to remove the unreacted ester **4**. The water layer was acidified with 20% HCl and extracted with EtOAc. The organic extracts were washed with saturated solution of NaCl, dried with Na₂SO₄ and evaporated *in vacuo*. TLC purification (CH₂Cl₂ : EtOAc = 1 : 1; $R_f = 0.23$) gave the desired product as an orange powder on the removal of the solvent *in vacuo* (297.5 mg, 62%); mp 128-134 °C; IR (CH₂Cl₂): $\nu_{\max}/\text{cm}^{-1} = 3420$ (w, NH_{free}), 3296 (m, NH_{assoc}), 3109-2800 (m, OH, COOH), 1710, 1697, 1653 (s, C=O_{COOH}, CONH), 1576 (amide II); ¹H NMR (600.133 MHz; CD₃OD; Me₄Si): δ (ppm) = 4.71 (s, 1H, H_{Fn}), 4.66 (s, 2H, H_{Fn}), 4.52-4.48 (m, 2H, H_{Fn}, CH_{Ala}), 4.29 (s, 1H, H_{Fn}), 4.27 (s, 1H, H_{Fn}), 4.01 (m, 2H, H_{Fn}), 2.05 (s, 3H, CH_{3Ac}), 1.36 (d, $J = 5.6$ Hz, 3H, CH_{3Ala}); ¹³C NMR, APT (150.917 MHz; CD₃OD; Me₄Si): δ (ppm) = 173.67 (CO_{Fn}, CO_{COOH}, CO_{Ac}), 95.67, 79.51 (C_{qFn}), 72.83, 72.38, 72.13, 67.04, 66.93, 64.46, 64.42 (CH_{Fn}), 50.98 (CH_{Ala}), 22.66 (CH_{3Ac}), 18.03 (CH_{3Ala}); ESI-MS (H₂O : MeOH = 50 : 50): $m/z = 381.1$ [(M+Na)⁺].

Synthesis of Ac-Ala-NH-Fn-NHBoc (7)

Carbamate **7** was prepared starting from acid **5** *via* unstable azide **6**. Acid **5** (130 mg, 0.36 mmol) was suspended in water (0.1 ml) and sufficient acetone was added to complete the solution. After cooling to 0 °C, triethylamine (42 mg, 0.41 mmol) in acetone (0.65 ml) was added. While maintaining the temperature at 0 °C, a solution of ethyl chloroformate (49.2 mg, 0.45 mmol) in the same solvent (0.2 ml) was added and the mixture was stirred for 30 min at 0 °C. Thereafter, a solution of sodium azide (35.3 mg, 0.54 mmol) in water (0.1 ml) was added. The mixture was stirred for 1 h (0 °C) and acetone was removed *in vacuo* to leave crude unstable azide **6**, which was converted *in situ* to carbamate **7** by heating with dry *t*-BuOH (5 ml) at 65 °C for 5 h. The reaction mixture was evaporated to dryness and purified by preparative chromatography in EtOAc ($R_f = 0.33$) giving yellow powder of **7** (60 mg, 39%); mp 142-145 °C; IR (CH₂Cl₂): $\nu_{\max}/\text{cm}^{-1} = 3428$ (s, NH_{free}), 3313 (w, NH_{assoc}), 1703 (s, C=O_{Boc}), 1682, 1665 (s, C=O_{CONH}), 1530,

1513 (amide II); ¹H NMR (600.133 MHz; CDCl₃; Me₄Si): δ (ppm) = 8.30 (s, 1H, NH_{Fn}^a), 6.58 (d, $J = 7.5$ Hz, 1H, NH_{Ala}), 6.23 (s, 1H, NH_{Boc}), 4.61-4.53 (m, 3H, H_{Fn}, CH_{Ala}), 4.35-4.30 (m, 2H, H_{Fn}), 4.13-4.01 (m, 4H, H_{Fn}), 2.05 (s, 3H, CH_{3Ac}), 1.50 [s, 9H, (CH₃)₃Boc], 1.44 (d, $J = 6.9$ Hz, 3H, CH_{3Ala}); ¹³C NMR, APT (150.917 MHz; CDCl₃; Me₄Si): δ (ppm) = 171.20 (CO_{Fn}), 170.54 (CO_{Ac}), 80.54 (C_{qBoc}), 65.93, 65.53, 65.47, 65.15, 62.95 (CH_{Fn}), 49.51 (CH_{Ala}), 28.55 [(CH₃)₃Boc], 23.37 (CH_{3Ac}), 18.43 (CH_{3Ala}); ESI-MS (H₂O : MeOH = 50 : 50): $m/z = 452.2$ [(M+Na)⁺].

Synthesis of Ac-Ala-NH-Fn-NH-Ala-Boc (3b)

Carbamate **7** (500 mg, 1.16 mmol) was suspended in CH₂Cl₂ (3 ml) and HCl gaseous was bubbled through the suspension for 30 min at 0 °C. The obtained hydrochloride salt was suspended in CH₂Cl₂ and treated with NEt₃ to give unstable free base which was coupled with Boc-Ala-OH (440 mg, 2.33 mmol) using standard EDC/HOBt method [EDC (533.6 mg, 2.78 mmol); HOBt (375.3 mg, 2.78 mmol)]. The reaction mixture was stirred at room temperature until complete consumption of the ferrocene starting material, as monitored by TLC. The standard work-up (washing with a saturated aqueous solution of NaHCO₃, 10% aqueous solution of citric acid and brine, drying over Na₂SO₄ and evaporation *in vacuo*) followed with TLC purification of the crude products (EtOAc; $R_f = 0.51$) gave orange crystals of the desired product (408 mg, 70%); mp 141-143 °C; IR (CH₂Cl₂): $\nu_{\max}/\text{cm}^{-1} = 3439$ (w, NH_{free}), 3310, 3253 (m, NH_{assoc}), 1684, 1665 (s, C=O_{CONH}), 1571, 1506 (amide II); ¹H NMR (600.133 MHz; CDCl₃; Me₄Si): δ (ppm) = 9.09 (s, 1H, NH_{Fn}^a), 9.06 (s, 1H, NH_{Fn}^b), 6.85 (d, $J = 5.2$ Hz, 1H, NH_{Ala}^a), 5.36 (s, 2H, H-10, H-7), 5.21 (d, $J = 6.3$ Hz, 1H, NH_{Ala}^b), 4.58 (dq, $J = 8.0$ Hz, 7.1 Hz, 1H, CH_{Ala}^a), 4.24 (dq, $J = 8.0$ Hz, 7.1 Hz, 1H, CH_{Ala}^b), 4.14 (s, 1H, H-2), 4.09 (s, 1H, H-5), 3.96 (s, 4H, H-3, H-4, H-8, H-9), 2.11 (s, 3H, CH_{3Ac}), 1.46 [s, 9H, (CH₃)₃Boc], 1.39 (d, $J = 6.9$ Hz, 3H, CH_{3Ala}^a), 1.36 (d, $J = 6.7$ Hz, 3H, CH_{3Ala}^b); ¹³C NMR, APT (150.917 MHz; CDCl₃; Me₄Si): δ (ppm) = 171.94 (CO_{Fn}^a), 171.67 (CO_{Fn}^b), 171.45 (CO_{Ac}), 156.80 (CO_{Boc}), 96.16 (C-1), 95.69 (C-6), 80.81 (C_{qBoc}), 65.86 (C-8), 65.78 (C-9), 64.90 (C-3), 64.82 (C-4), 62.83 (C-7), 62.75 (C-10), 61.65 (C-2), 61.25 (C-5), 51.14 (CH_{Ala}^b), 50.31 (CH_{Ala}^a), 28.54 [(CH₃)₃Boc], 23.08 (CH_{3Ac}), 17.84 (CH_{3Ala}^b), 17.45 (CH_{3Ala}^a); MALDI-HRMS $m/z = 500.1726$ (calculated for C₂₃H₃₂N₄O₅Fe = 500.1717).

Synthesis of Ac-Ala-NH-Fn-NH-Ala-Ac (3c)

The transformation of orthogonally protected peptide **3b** (400 mg, 0.8 mmol) to Ac-analogue **3c** was carried out by action of acetyl chloride (315 μ L, 4.8 mmol): the free base, obtained *via* hydrochloride salt provided by deprotection of **3b** in the above described manner, was cooled at 0 °C and acetyl chloride was dropwise added. After stirring in an ice bath for 15 min, TLC indicated no residual starting material remained and the reaction mixture was poured into water and extracted with CH₂Cl₂. The combined organic phases were washed with a brine, dried over Na₂SO₄ and evaporated to dryness *in vacuo*. The resulting crude product was purified by TLC on silicagel (*n*-BuOH : CH₃COOH : H₂O = 60 : 25 : 15; $R_f = 0.64$) to give

orange solid of **7** (325 mg, 92%); mp 112–114 °C; IR (CH₂Cl₂): $\nu_{\text{max}}/\text{cm}^{-1}$ = 3438 (w, NH_{free}), 3306, 3252 (m, NH_{assoc.}), 1686, 1678, 1665, 1650 (s, C=O_{CONH}), 1570 (amide II); ¹H NMR (300 MHz; CDCl₃; Me₄Si): δ (ppm) = 8.98 (s, 2H, NH_{Fn}), 6.19 (d, J = 5.2 Hz, 2H, NH_{Ala}), 5.23 (s, 2H, H-10, H-7), 4.50 (m, 2H, CH_{Ala}), 4.11 (s, 2H, H-2, H-5), 3.96 (s, 4H, H-3, H-4, H-8, H-9), 2.09 (s, 6H, CH_{3Ac}), 1.41 (d, J = 6.9 Hz, 6H, CH_{3Ala}); ¹³C NMR, APT (75.432 MHz; CDCl₃; Me₄Si): δ (ppm) = 171.40 (CO_{Fn}), 171.37 (CO_{Ac}), 95.56 (C-1, C-6), 65.79, 64.83 (C-3, C-4, C-8, C-9) 63.08, 61.82 (C-2, C-5, C-7, C-10), 50.35 (CH_{Ala}), 23.23 (CH_{3Ac}), 17.63 (CH_{3Ala}); MALDI-HRMS m/z = 442.1291 (calculated for C₂₀H₂₆N₄O₄Fe = 442.1298).

X-Ray determination of **3b**

The orange prismatic crystal with dimensions 0.79×0.36×0.14 mm³ was obtained at room temperature by partial evaporation from a chloroform solution. The intensities were collected at 295 K on Oxford Diffraction Xcalibur 2 diffractometer using graphite-monochromated MoK α radiation (λ = 0.71073 Å). The *CrysAlisPro*¹⁴ program was used for the data collection and processing. The intensities were corrected for absorption using the multi-scan absorption correction method.¹⁴ The structure was solved by direct methods with *SIR-2004*¹⁵ and refined by full-matrix least-squares calculations based on F^2 using *SHELXL-2013*¹⁶ integrated in the *WinGX*¹⁷ program package. Hydrogen atoms attached to the nitrogen atoms (N1–N4) have been found in the difference Fourier maps and their isotropic thermal parameters have been refined freely. Geometric restraint on N–H distance was applied in the refinement. All other hydrogen atoms were included in calculated positions as riding atoms, with *SHELXL-2013*¹⁶ defaults. *PLATON*¹⁸ program was used for structure analysis and molecular and crystal structure drawings preparation. CCDC 1060677 contains the supplementary crystallographic data for this paper. These data can be obtained free of charge from The Cambridge Crystallographic Data Centre via www.ccdc.cam.ac.uk/data_request/cif.

Crystal data for **3b**: C₂₄H₃₃Cl₃FeN₄O₅, M_r = 619.74, orthorhombic space group $P2_12_12_1$ (No. 19); a = 8.9475(4), b = 16.3934(11), c = 20.8167(17) Å; V = 3053.4(4) Å³; Z = 4; d_x = 1.348 g cm⁻³; μ = 0.794 mm⁻¹; R_{int} = 0.0344; x = -0.010(12); S = 0.981; R/wR = 0.0630/0.1550 for 356 parameters and 4443 reflections with $I \geq 2\sigma(I)$, R/wR = 0.1007/0.1803 for all 6637 independent reflections measured in the range 4.37°– θ -27.00°.

Computational details

Geometries of the selected compounds were analysed with MacroModel v10.3^{19,20,21} using several different search methods with OPLS_2005 force field.²² A ferrocene unit was frozen during optimization. Restrictions were imposed on pseudo-torsion angle during conformational search, thus simulating rotation of two Cp rings. Conformers were then optimized with Gaussian09 (Revision D.01)²³ at the B3LYP-D3/LanL2DZ level of theory using Grimme's dispersion with the original D3 damping function.^{24,25,26} The most stable conformers were reoptimized in chloroform at B3LYP-D3/6-311+G(d,p) level of theory, using IEF-PCM for describing

implicit solvent effects.^{27,28} Iron was modelled using ECP set LanL2DZ. Molecules were visualized using Chem3D 2012²⁹ and GaussView 5³⁰ programs. AIM2000 program were used for the topological analysis of selected compounds.^{31,32} Hirshfeld surface analysis^{33,34} was performed with CrystalExplorer.³⁵

Biological evaluation

Cell culture. Hep G2 (human liver carcinoma cells; ATCC® HB-8065™) and Hs 578T (human breast cancer cells; ATCC® HTB-126™) cell lines were purchased from American Type Culture Collection (ATCC, USA). Hep G2 cells were maintained in Dulbecco's Modified Eagle Medium Nutrient Mixture F-12 with 15 mM HEPES buffer and L-glutamine (DMEM/F-12 (1:1); Gibco, Paisley, UK) and Hs 578T cells were cultivated in ATCC-formulated Dulbecco's Modified Eagle's Medium (DMEM, ATCC, USA) with supplemental bovine insulin (0.01 mg/mL) (Sigma-Aldrich, St Louis, MO). Heat inactivated Fetal Bovine Serum (Gibco, Paisley, UK) was added to make the complete growth medium for both cell lines in final concentration of 10%. Cells were routinely cultured in 80 cm² cell flasks (Nunc, Roskilde, Denmark) at 37° C and humidified in atmosphere of 5% CO₂ in air. After reaching 70–90% confluence the cells were disaggregated using a trypsin/EDTA (0.25% trypsin, 1mM EDTA-4Na), counted and placed at the necessary density prior to sub-culture or seeding in wells for experimental needs.

Treatment. Cells in log phase of growth were seeded in 96-well plates (100 μ L of cell solution per well) at the initial concentration of 5×10⁴ cells/mL and allowed 24 h to attach before treatment with ferrocene and tested compounds **2a**, **3b** and **3c**. Stock solutions of ferrocene and tested compounds **2a**, **3b** and **3c** were prepared as 10 mM solutions in ethanol (EtOH) and stored at 4° C. Prior to use in cytotoxicity assay, the stock solutions were further diluted with culture medium to obtain the desired final concentrations (50 – 500 μ M). The media was replaced with fresh one containing different concentrations of individual test compound. Cytotoxic effects were evaluated after 72 h of exposition. Samples with ethanol without tested compounds were used as controls. Final concentration of ethanol did not exceed 0.5% and had no interference with the biological activities tested.

MTT Cytotoxicity Assay. The cytotoxicity of ferrocene and tested compounds **2a**, **3b** and **3c** was determined by MTT assay.³⁶ The cells were incubated with tetrazolium salt MTT [3-(4,5-dimethylthiazol-2-yl)-2,5-diphenyltetrazolium bromide] for 4 h. The absorbance was measured at 570 nm on the microplate reader (model LKB 5060-006, LKB Vertriebs GmbH, Vienna, Austria). The experiments were performed three times with four parallels for each concentration and data were expressed as the means \pm SEM. Cell viability was expressed as percentage of treated cells vs. control cells. The IC₅₀ values, defined as the concentration of tested compound that results with 50% growth inhibition, were derived from the equations of related trend lines.

Statistical Analysis. A two-tailed Student's t-test was applied to evaluate the significant differences between control and

treated cells. The results are reported as means \pm SEM, $p < 0.05$ was considered significant.

Results and discussion

Synthesis of bioorganometallics **3b** and **3c**

The key intermediate **7**, containing NH groups attached to both Cp rings, was obtained from Ac-Ala-Fca-OMe (**4**).¹³ In order to prevent racemisation of its chiral center, the saponification of ester group of compound **4** was performed with an equimolar amount of base under restricted conditions (1h/ 80°C). The resulting compound **5** was transformed to unstable azide **6** that was *in situ* subjected to Curtius rearrangement by heating in *t*-BuOH to give orthogonally protected compound **7**. In order to avoid the undesired conversion of the intermediate isocyanate group to the corresponding urea, *t*-BuOH was dried before use and the rearrangement temperature was limited to 65 °C. Otherwise, the temperature increment led to the formation of sym-urea derivative. Since TLC monitoring did not show any difference between isocyanate intermediate and the azide precursor **6**, the completing of the reaction was confirmed by complete absence of the azide and isocyanate bands (2130 cm^{-1} and 2270 cm^{-1}) in IR spectrum of the crude reaction mixture. Boc-deprotection of **7** was conducted in acidic milieu, leaving Ac protective group at upper Cp intact. The obtained Ac-Ala-NH-Fn-NH₂-HCl was processed with an excess of NEt₃ to liberate the *N*-terminus, followed by coupling with activated Boc-Ala-OH to give orthogonally protected Ac-Ala-NH-Fn-NH-Ala-Boc (**3b**). Upon (i) Boc-deprotection and (ii) Ac-protection in the presence of acetyl chloride,³⁷ Fn-(NH-Ala-Ac)₂ (**3c**) was obtained (Scheme 1).

Conformational analysis of **3b** and **3c** in solution

Herein presented facile and efficient strategy for the preparation of novel bioorganometallics **3** containing peptide sequences of different structure and chirality attached at N-H functionalized Cp rings has been applied for the synthesis of their lowest homologues **3b** and **3c**. Considering that both carbamate carbonyl groups of their Kraatz's analogue **3a**¹¹ have been engaged in strong IHBs forming 14-membered ring in solution as well as in the solid state, we wanted to explore if the replacement of one or both bulky Boc groups with Ac function will influence the IHB pattern, because of the decreasing steric hindrance. For this purpose, the spectral data of bioorganometallics **3b** and **3c** are compared to those related to the model (**3a**¹¹, **10**³⁸, **11**^{10b} and **12**³⁸) and reference compounds (**8** and **9**)^{10b} (Fig. 2). The model compounds were chosen due to their structural and hydrogen-bonding ability similar to those of the analysed peptides, while the reference compounds are characterized by inability to form IHBs.

Our endeavor to clarify the conformational properties of **3b** and **3c** began with IR analysis (Table 1). The two clearly

Table 1 IR (ν in cm^{-1}) and NMR (δ in ppm)^[a] spectroscopic data of reference (**8** and **9**), model (**3a**, **10-12**) and goal compounds (**3b** and **3c**).

Compound	ν_{NH}		ν_{CO} Amide I	δ			NH_{Ac}
	Free	Assoc. [b]		$\text{NH}_{\text{Fn}}^{\text{a}}$	$\text{NH}_{\text{Fn}}^{\text{b}}$	NH_{Boc}	
3a				9.00	5.11		
3b	3439	3310 3253	1684 1665	9.06	9.02	5.21	6.85
3c	3438	3306 3252	1686 1678 1665 1650	9.04			6.57
8	3436		1723	5.55			
9	3436		1684	6.49			
10	3425	3336	1697	5.55	6.83		
11	3431	3328	1711 1687	7.41		5.80	
12	3428	3328	1710 1679	7.88	8.14	5.52	

[a] IR and NMR spectra were recorded in CH_2Cl_2 ($c = 5 \times 10^{-2}$ M).

[b] No solution data available.

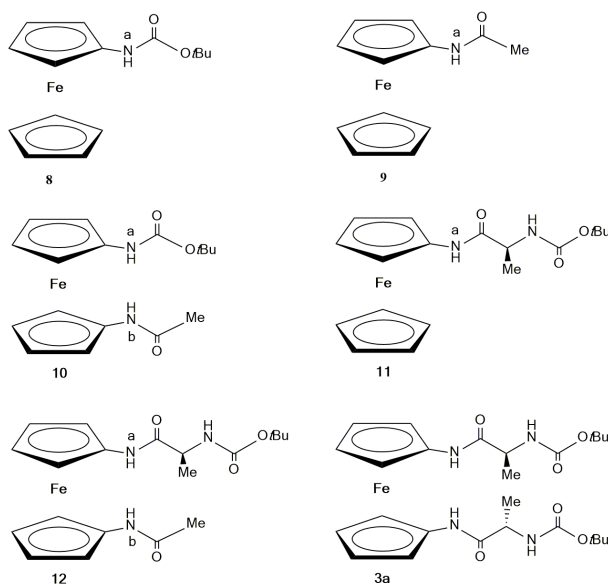


Figure 2. The reference (**8** and **9**) and model compounds (**10-12**, **3a**).

distinct NH absorptions are indicative of two-state equilibrium between non-bonded ($> 3400 \text{ cm}^{-1}$) and hydrogen-bonded conformations ($< 3400 \text{ cm}^{-1}$). The hydrogen bonding behaviour of the NH groups of **3b** dominates this region of the spectra and is evidently independent on concentration (Fig. 3) and clearly intramolecular in nature [the ratio of the associated and free NH bands (1.8 : 1) did not change during the course of the experiment]. A closer inspection of Fig. 3 revealed that

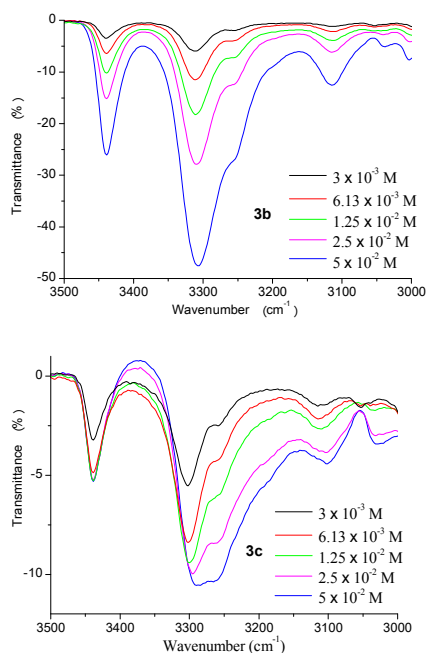


Figure 3. The NH stretching vibrations in concentration-dependent IR spectra of **3b** and **3c** in CH_2Cl_2 .

intensity of free NH bands of **3c** remained unchanged upon dilution from 5×10^{-2} M to 1.25×10^{-2} M as opposed to the corresponding associated NH bands which were reduced up to 11%. Nevertheless, the proportion of hydrogen-bonded and free NH bands of **3c** persisted unchanged (1.74 : 1) during further dilution. This data proved the predominance of the intramolecular HBs, but also the existence of the intermolecularly bonded NH groups of **3c**.

Although our previous studies of ferrocene peptides revealed the considerable interference of bulky Boc group with hydrogen bonding,^{13,39} the similar ratios of hydrogen-bonded and non-bonded NH peak intensities in IR spectra of **3b** and **3c** exclude the sterical hindrance of Boc group. Taking into account that (i) hydrogen-bond-accepting urethane⁴⁰ and acetamide group^{10d} appear at lower wavenumbers and (ii) urethane and acetamide carbonyl groups of **3b** and **3c** are shifted to the lower region in comparison to non-bonded reference compounds **8** and **9**, their engagement in hydrogen bonding is suggested. Thereby, non-bonded urethane carbonyl groups of the model compounds **11** and **12** absorb at higher wavenumbers.

The next step in the evaluation of the conformational preferences of the bioconjugates **3b** and **3c** in solution is interpretation of their NMR spectra. Indeed, all the amide protons resonances were recognized by analysis of coupling patterns and two-dimensional NMR spectra. [Due to the presence of the multiple resonances in the NMR spectra (Fig. S25, Fig. S27), one can assume that peptide **3c** tends to partially aggregate in concentrated solution (50 mM),⁴¹ as it was

observed by IR spectroscopy. Upon dilution of the NMR sample, these resonances underwent complete coalescence, (Fig. S26, S28, S29)]. The dependence of the amide chemical shifts on the accessibility of the proton to the hydrogen-bond accepting site is well documented.⁴² The downfield chemical shifts ($\delta \geq 7$ ppm) in non-polar CDCl_3 are generally considered to be assigned to the hydrogen-bonded NH protons. Herein, the resonances of NH_{Fn} at ~ 9 ppm match very closely with those observed for the intramolecularly hydrogen-bonded amide proton of the model peptide **3a**. Conversely, NH_{Boc} and NH_{Ac} displayed the lowering of the chemical shift values compared to the amide group attached at ferrocene core suggesting a lowered potential to experience IHBs. Furthermore, the correlation of NH_{Boc} and NH_{Ac} chemical shifts of the examined peptides **3b** and **3c** with those observed for the non-bonded carbamate and acetamide groups of **8-12** does not support the possible hydrogen bond donating engagement of alanine moieties (Table 1).

In order to gain more insight into the conformational behaviour of these bioorganometallics, the concentration- and temperature-dependent NMR measurements were carried out. Since no significant concentration-dependent changes in chemical shifts of NH_{Fn} were seen ($\Delta\delta = 0.06\text{-}0.13$ ppm), their participation in intramolecular HB is further supported (Fig. 4, Fig. S17, Fig. S29). The successive dilution did not considerably affect the chemical shift of non-bonded NH_{Boc} proton of **3b** ($\Delta\delta = 0.13$ ppm), while NH_{Ac} protons of **3b** and **3c** experienced more appreciable upfield shifts ($\Delta\delta \geq 0.4$ ppm), which might account for their involvement to a lesser extent in intermolecular HB.

Amide proton temperature coefficients ($\Delta\delta/\Delta T$) are useful for the prediction of hydrogen bonding ability.⁴³ Since ferrocene peptides are subjected to rapid decomposition in DMSO, their temperature dependences, *i.e.* exposure or shielding of NH groups to solvent, were measured in CDCl_3 .^{13,39,44} Low $\Delta\delta/\Delta T$ values (-2.4 ± 0.5 ppb/K) correspond to both exposed and shielded amide protons of short peptides and thus are not very informative. The larger temperature dependencies are interpreted as indication of initially shielded NH groups that became exposed to solvent upon dissociation of the self-associated aggregates or unfolding of ordered conformations at increased temperatures.⁴⁵ Therefore, the low $\Delta\delta/\Delta T$ value of non-bonded NH_{Boc} proton is attributed to its exposure to solvent, while unfolding as well as dissociation lead to increased temperature dependences of initially shielded NH_{Fn} and NH_{Ac} , respectively (Fig. 5, Fig. S18, Fig. S30).

Hydrophobic and hydrogen bonding interactions are of fundamental importance for the folding and misfolding behaviour of proteins.⁴⁶ We decided, therefore, to investigate the hydrogen-bonding features of novel bioorganometallics by DMSO titration.⁴⁷ DMSO is well-known to display a strong



Journal Name

ARTICLE

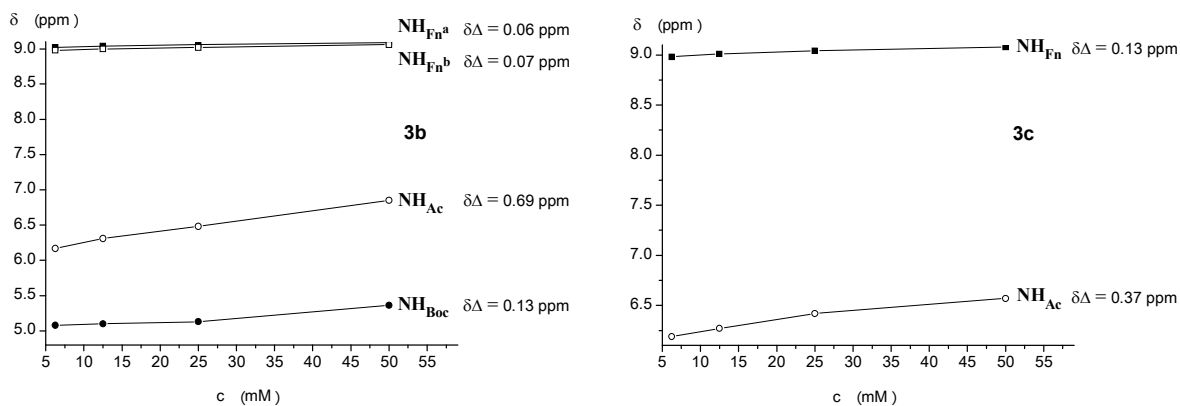


Figure 4. Concentration dependent NH chemical shifts of peptides **3b** and **3c**. [$^1\text{H-NMR}$ measurements were performed for a series of 6.25, 12.5, 25 and 50 mM solutions].

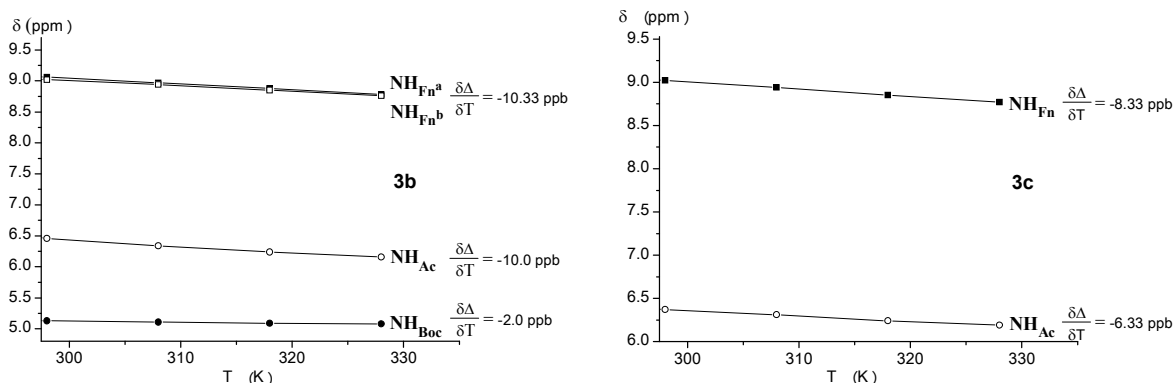


Figure 5. Temperature dependent NH chemical shifts of peptides **3b** and **3c** ($c = 2.5 \times 10^{-2}$ M) in the temperature range of 298–328 K.

tendency to accept amide NH protons exposed to solvent thereby causing the downfield shifts. If the amide protons are inaccessible to DMSO due to their engagement in HBs, no significant changes in chemical shifts will be observed. The conservation of high chemical shift values of NH_{Fn} protons upon titration with DMSO ($\Delta\delta < 0.2$ ppm) indicates their participation in a strong IHB. In contrast, carbamate and acetamide NH protons experienced a significant modulation of chemical shifts ($\Delta\delta > 1.7$ ppm), confirming the proposed non-hydrogen-bonded state for NH_{Boc} as well as involvement of NH_{Ac} in a weak HB (Fig. 6, Fig. S19, Fig. S31).

All these considerations on hydrogen-bonding behaviour of our peptides contribute to defining their conformational space based on interchain $\text{NH}_{\text{Fn}} \cdots \text{OC}_{\text{Boc/Ac}}$ IHBs. The NOE contact between NH_{Fn} linked at one Cp ring and *t*Bu group belonging to the chain attached to another Cp ring supports the proposed interchain intramolecular hydrogen bonding engagement with the carbamate carbonyl group (Fig. 7).

It was shown that hydrogen bonding between podand chiral peptide chains of the previously reported ferrocenes **1-3a** provokes chirality-organized structures detected by CD spectroscopy. The observed strong Cotton effects ($M_{\theta} \sim 5000 \text{ deg cm}^2 \text{ dmol}^{-1}$ for peptides **1** and $M_{\theta} \sim 10000 \text{ deg cm}^2 \text{ dmol}^{-1}$ for peptides **2**) in the region of ferrocene-based transitions around 470 nm were ascribed to highly organized chiral surrounding around ferrocene unit.⁴⁸ In addition, the earlier described L-Ala containing bioorganometallics **1**, **2** and **3a** displayed the positive Cotton effect attributed to the right-handed helicity. Considering that Cotton effect reflects an average of the entire molecular population, the domination of *P*-helicity of herein studied peptides **3b** and **3c** is strongly supported, owing to their pronounced CD activity. DMSO, a potent hydrogen bond acceptor, is capable to disrupt the weak hydrogen bonds and thereby jeopardize the conformational stability.^{10a,10d,10e} The CD-data obtained upon treatment of

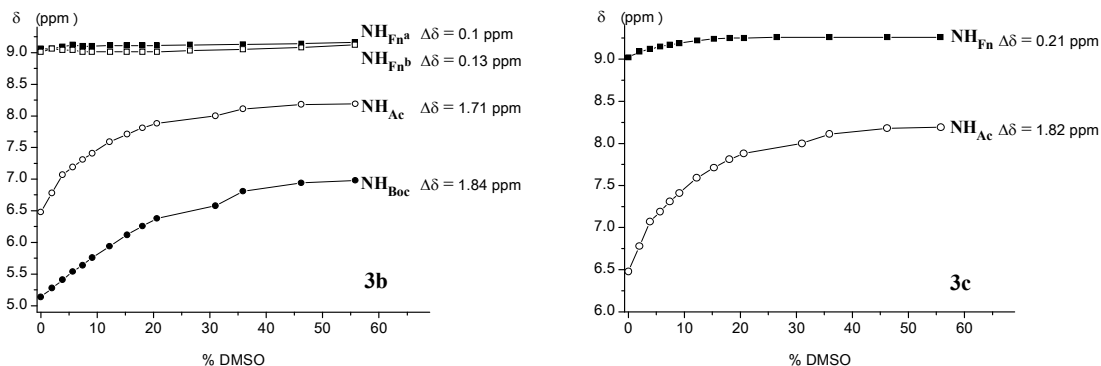


Figure 6. Solvent dependence of NH chemical shifts of **3b** and **3c** at varying concentrations of d_6 -DMSO in CDCl_3 ($c = 2.5 \times 10^{-2}$ M, 298 K) to probe exposed vs. hydrogen-bonded amides.

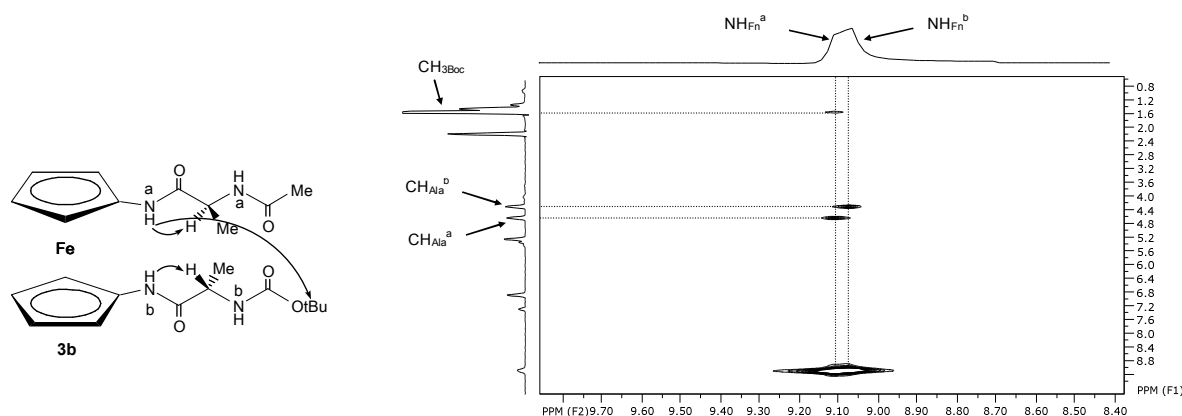


Figure 7. The interchain NOE connectivity between NH_{Fn} and $t\text{Bu}$ group of **3b** is depicted with arrows.

peptides **3b** and **3c** with 20% of DMSO determined the conservation of $\sim 70\%$ of the DMSO-free CD activity, certainly due to the existence of a strong IHBs (Fig. 8).

The peptides **3a-3c** containing ferrocene-1,1'-diamine (Fcda) and Ala was shown to adopt a conformation defined by 14-membered IHB-ring, resembling the hydrogen bonding in a antiparallel β -sheet peptides. Since side-chain groups affect the backbone folding,⁴⁹ our future work on ferrocenes **3** will include the replacement of one Ala unit with different amino acids to get a small library of Fcda-derived peptides. Those simple model systems will enable us to determine the amino acids predisposed to get involved in the β -turn-mediated folding of peptides **3**.⁵⁰ Besides that, we will elongate the N -termini of the lowest homologues **3a-3c** in order to establish models for extended β -sheet-like structures.

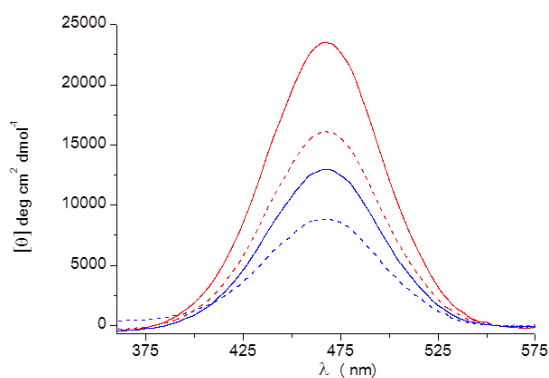


Figure 8. The Cotton effects in chirality-organized ferrocene peptides [CH_2Cl_2 ($c = 5 \times 10^{-3}$ M), (— **3b**, — **3c**) and CH_2Cl_2 ($c = 5 \times 10^{-3}$ M) containing 20% of DMSO (--- **3b**, --- **3c**)].

X-ray crystal structure analysis of **3b**

An orange crystal of the ferrocene derivative **3b** was grown at room temperature from chloroform solution and it crystallised in the chiral orthorhombic space group $P2_12_12_1$ as chloroform solvate. The absolute configuration of the stereogenic carbon atoms C12 and C20 of the L -Ala substituents is, as expected, S (Fig. 9).

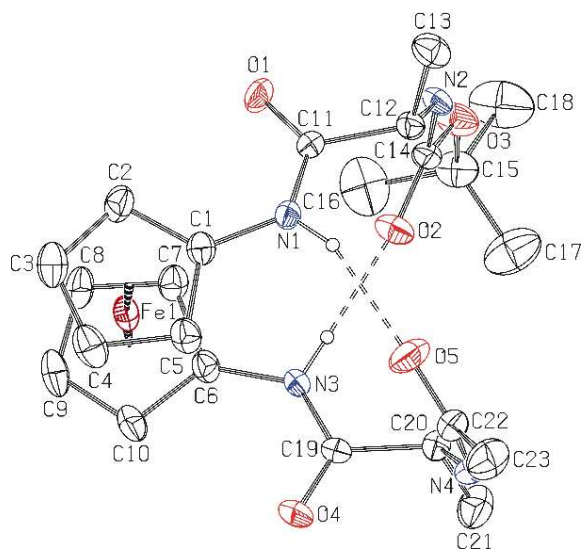


Figure 9. A molecular structure of **3b**, with the atom numbering scheme, showing $\text{N-H}\cdots\text{O}$ intramolecular hydrogen bonds (indicated by dashed lines). Displacement ellipsoids for nonhydrogen atoms are drawn at the 20% probability level. Chloroform

molecule and hydrogen atoms not included in intramolecular hydrogen bonds have been omitted for clarity.

The bond lengths in the two peptide strands attached to the cyclopentadienyl (Cp) rings, as well as within the ferrocene core, present no unexpected features and agree well with equivalent ones in **3a**.¹¹

The pseudo C1–Cg1–Cg2–C6 torsion angle of the ferrocene (Cg1 is centroid of the ring C1–C5 and Cg2 is centroid of the ring C6–C10) amounts to *ca.* +41°, *i.e.* a positive helical chirality (*P*) is observed. The value of this torsion angle also shows that conformation of the ferrocene is 1,2', and that cyclopentadienyl (Cp) rings adopt staggered conformation. The Cp rings are nearly coplanar to each other, with a tilt angle of 4.5(5)°.

The direction of the 1- and 1'-substituents of **3b** is a consequence of intramolecular (IHB) N–H···O hydrogen bonds that link the juxtaposed strands. These IHBs are formed between amide N–H groups and carbonyl oxygen atoms (Fig. 9, Table 2). The N1···O5 and N3···O2 hydrogen bonds form ten-membered rings of the $R_1^1(10)$ type,⁵¹ thus inducing a β -turn as in our previous published structure.⁵² In addition, the combination of these two IHBs form a new ring of the $R_2^2(14)$ type. Because of the above mentioned IHBs, the non-hydrogen atoms of amide groups attached to Cp rings, N1/C11/O1, *i.e.* N3/C19/O4, are twisted for 17.7(8) and 11.5(9)° with respect to the mean planes of C1–C5 and C6–C10 ring atoms, respectively. In **3b**, three intramolecular C–H···O hydrogen contacts are also observed (C2···O1, C16···O2 and C17···O2).

In the crystal, the molecules of **3b** are self-assembled by two N–H···O hydrogen bonds, N2···O1 and N4···O4, both of them linking molecules into infinite *zig-zag* C(5) chains⁵¹ parallel to the *a* axis. The combination of these two chains generates sheets and leads to a (4,4) net⁵³ (Fig. 10a). Chloroform molecules fill the gaps between the hydrogen-bonded molecules of **3b** (Fig. 10b), and are linked to the ferrocene molecules by one C–H··· π interaction (C24···Cg1, Table 2). Crystal packing diagram along the *a* axis reveals that hydrogen atoms of chloroform molecules point to the Cp rings of **3b**, thus also participating in the formation of two-dimensional network (Fig. 10b).

Computational study of **3a**, **3b** and **3c**

Our previously published papers about the conformational analysis of ferrocene containing peptides have resulted in close agreement between experimental and DFT calculated data.^{13,48,54} Herein, we have decided to use the same approach to

Table 2. Hydrogen-bonding geometry for **3b**.

D–H···A	D–H (Å)	H···A (Å)	D···A (Å)	D–H···A (°)
N1–H···O5	0.86(5)	2.06(5)	2.859(7)	156(4)
N3–H···O2	0.86(5)	1.95(5)	2.802(7)	175(6)
C2–H···O1	0.93	2.58	2.976(8)	106
C16–H···O2	0.96	2.58	3.040(14)	110
C17–H···O2	0.96	2.33	2.975(13)	124
N2–H···O1	0.86(5)	2.00(5)	2.851(7)	174(6) ^a
N4–H···O4	0.86(4)	2.01(5)	2.851(7)	166(7) ^b
C24–H···Cg1 ^c	0.98	2.78	3.726(11)	162

Symmetry codes: ^[a] –1/2+x, 3/2–y, 1–z; ^[b] –1/2+x, 1/2–y, 1–z.

^[c] Cg1 is centroid of the C6–C10 ring.

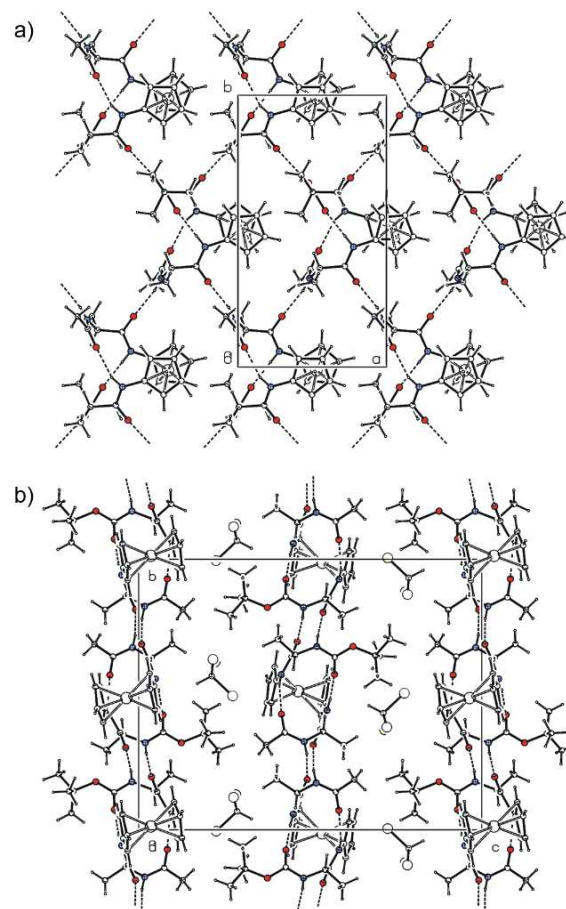


Figure 10. A crystal packing diagram of **3b**, viewed along the *c* axis (a) and the *a* axis (b), showing intramolecular and intermolecular N–H···O hydrogen bonds. Hydrogen bonds are indicated by dashed lines.

shed a light on hydrogen bond patterns observed in solution as well as in the solid state of the peptides **3a**, **3b** and **3c**. The combination of molecular and quantum mechanics approach has been used. The most stable conformers have been calculated with B3LYP-D3 functional and 6-311+G(d,p) basis set. Iron was described with LanL2DZ basis set. Chloroform was modelled as a polarizable dielectric continuum (IEF-PCM).

The generally accepted nomenclature of these and similar ferrocene containing compounds is displayed in Fig. 11. A

pseudo-torsion angle ω is used to describe rotation of two cyclopentadienyl rings. Depending on a relative value of the angle, the stereochemical descriptor $1,n'$ is usually assigned with *P*- and *M*- label. Modified *E/Z* marks are used to unambiguously determine relative orientation of Cp-amide bonds. All of the marked hydrogen bonds in Fig. 12 were confirmed by Bader's AIM theory. Values of topological parameters of the bond critical points between hydrogen-bond acceptor and hydrogen atom [electron density $\rho(r)$, Laplacian of the electron density $\nabla^2\rho(r)$ and the energy density $H(r)$] were determined and compared with the Koch and Popelier criteria

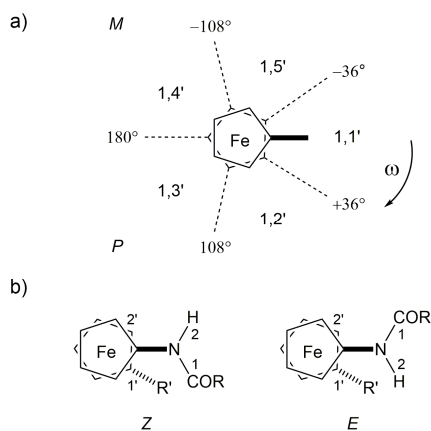


Figure 11. Nomenclature of $1,n'$ -disubstituted ferrocenes with chiral substituents. a) *M/P* isomers defined by a pseudo-torsion angle ω between two substituents; b) *E/Z* isomers describing an orientation of Cp-amide bond.

used to characterize hydrogen bonds.^{55,56} The results are presented in Table 3 and geometries of the most stable conformers are displayed in Fig. 12.

In this study both newly synthesized derivatives **3b** and **3c** as well as Kraatz's analogue **3a**¹¹ were subjected to conformational analysis. The results were very similar for all the three ferrocene conjugates. The engagement of NH_{Fn} in hydrogen bonding almost exclusively predominated in all of the conformers. In the most stable conformers (**3a-1**, **3b-1** and **3c-1**) the interchain $\text{NH}_{\text{Fn}} \cdots \text{OC}_{\text{Boc/Ac}}$ hydrogen bonds between two opposite substituents were the only one responsible for a folding of peptide chains. A 10-membered ring, also known as β -turn (IHB pattern A, Fig. 13) was formed. Consequently, methyl groups of each alanine pointed away from the place of interaction between substituents. Almost the same observation could be applied for the Boc and Ac groups, which also pointed away from the ferrocene. The most stable conformers of symmetrically substituted derivatives (**3a-1** and **3c-1**) adopted the C_2 point group.

In comparison with these conformers, in which another potential hydrogen bond donor group, *i.e.* NH_{Ala} , was not engaged in formation of any hydrogen bond, the second set of conformers (**3a-2**, **3b-2** and **3c-2**) utilized all of the

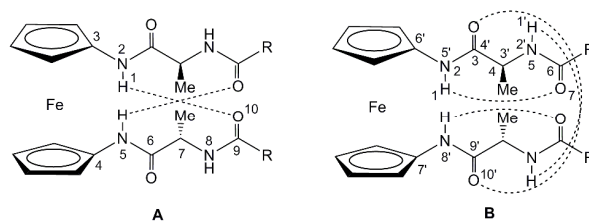


Figure 13. The hydrogen bond patterns (A and B) observed in the most stable conformers of **3a**, **3b** and **3c** in chloroform (PCM); R = Me, OrBu. Numerations of seven- and ten-membered rings are displayed.

available NH groups in formation of four hydrogen bonds. The observed IHB pattern B was constituted of two 7-membered rings (γ -turns) connected by intrachain $\text{NH}_{\text{Fn}} \cdots \text{OC}_{\text{Boc/Ac}}$ hydrogen bonds. Additionally, two opposite substituents were connected by two interchain $\text{NH}_{\text{Ala}} \cdots \text{OC}_{\text{Ala}}$ hydrogen bonds engaged in formation of 10-membered rings (β -turns). Again, conformers **3a-2** and **3c-2** with same substituents adopt the C_2 point group. The population of these conformers is more significant within **3b** and **3c** derivatives with sterically less demanding Ac group.

These results were compared with the experimental data. The calculated structure of the most stable conformer of **3b** also adopted (*P*) helical chirality with pseudo-torsion angle of *ca.* 28° , in comparison with 41° in X-ray determined crystal structure. The CD experiments in solution also confirmed the domination of (*P*) helical forms. According to NMR experiments, the full engagement of NH_{Fn} groups in intramolecular hydrogen bonds, while NH_{Boc} and NH_{Ac} groups are more prone to accomplish intermolecular hydrogen bonds, was also proven by the computational study.

Generally, hydrogen bonds can be related to a greater stabilization of conformers depending on specific IHB patterns. In our case, the NH groups of alanine residue remained non-hydrogen bonded in the most populated conformers. This observation is in agreement with X-ray determined structure of **3b**. Furthermore, these groups are able to form additional intermolecular hydrogen bonds as it is observed in crystal structure. Thus, we decided to investigate the effects of this interaction between two molecules of unsymmetrically substituted **3b** as the most appropriate model for further analysis.



Journal Name

ARTICLE

Table 3. Relative energies (in kJ mol^{-1}) of the most stable conformers of **3a-c** in chloroform at 298 K, stereochemical descriptors, pseudo-torsion angles (in $^\circ$) and IHBs patterns according to Fig. 13, X–Y distances (in \AA) of the selected X–H \cdots Y hydrogen bonds.

conformer	E_{rel}	stereochemical descriptors	ω pseudo-torsion angle	IHB pattern	NH _{Fn} \cdots OC _{Boc/Ac} (interchain)	NH _{Fn} \cdots OC _{Boc/Ac} (intrachain)	NH _{Ala} \cdots OC _{Ala} (interchain)
3a-1	0.00	(<i>P</i>)-1,1'; <i>E,E</i>	28.8	A	2.86 (2.86)	-	-
3a-2	9.23	(<i>M</i>)-1,5'; <i>Z,Z</i>	-59.0	B	-	3.03 (3.02)	2.91 (2.91)
3b-1	0.00	(<i>P</i>)-1,1'; <i>E,E</i>	28.3	A	2.86 (2.88)	-	-
3b-1	7.34	(<i>M</i>)-1,5'; <i>Z,Z</i>	-59.5	B	-	3.03 (2.99)	2.92 (2.89)
3c-1	0.00	(<i>P</i>)-1,1'; <i>E,E</i>	26.5	A	2.88 (2.88)	-	-
3c-2	5.50	(<i>M</i>)-1,5'; <i>Z,Z</i>	-60.3	B	-	2.98 (2.98)	2.90 (2.90)

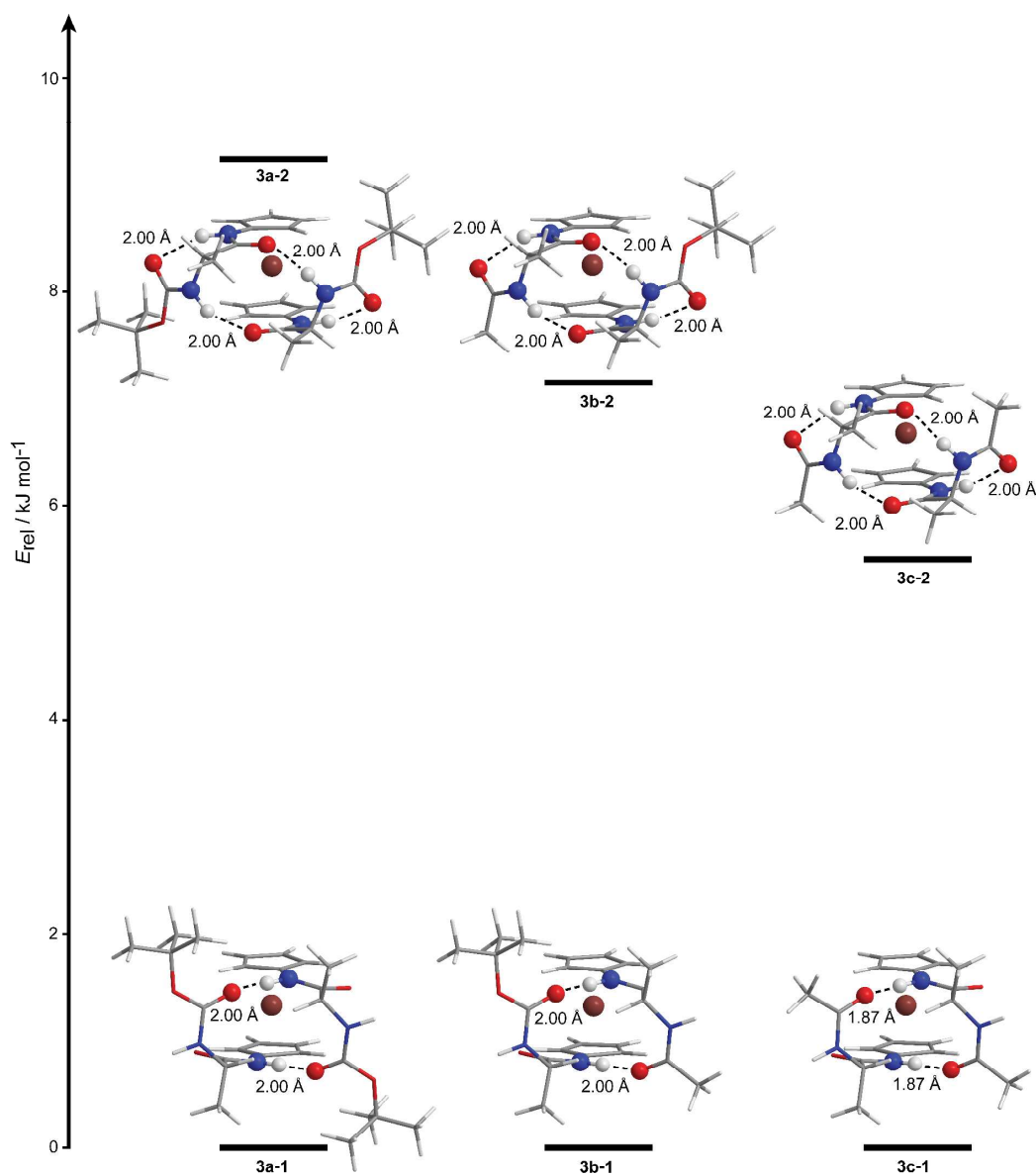


Figure 12. The most stable conformers of bioorganometallics **3a-e** with selected hydrogen bonds.

To gain better insight about close contacts we decided to employ Hirshfeld surface analysis. It summarizes the way in which one molecule interacts with neighbour molecules. Fig. 14a shows Hirshfeld surface mapped with d_{norm} values showing

distances shorter than the sum of the van der Waals radii (red spots). Obviously, both substituents, the first protected with Ac group (Fig. 14b), and the second protected with Boc group (Fig. 14c) interact in the same way with neighbouring molecules by



Journal Name

ARTICLE

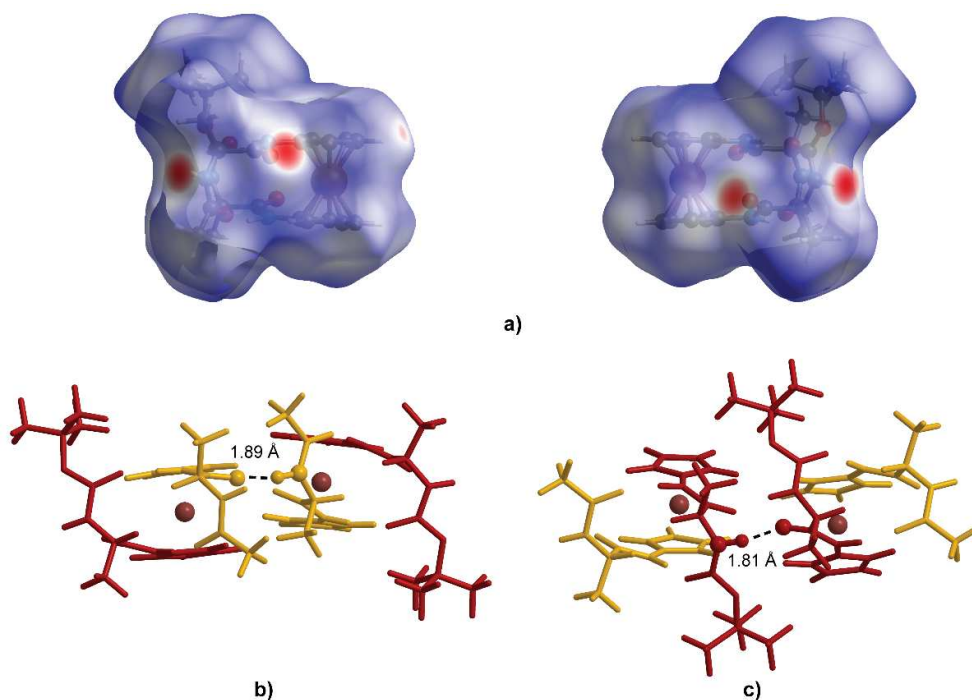


Figure 14. a) Hirshfeld surface of **3b** mapped with d_{norm} over the range -0.59 to 1.78 Å, areas with contact distances shorter than the sum of the van der Waals radii are coloured red. (left – look from the side of Ac protected substituent, right – look from the side of Boc protected substituent); b) Optimized geometry of **3b** pair of molecules connected through $NH\cdots O$ hydrogen bond between Ac protected substituents (coloured yellow); c) Optimized geometry of **3b** pair of molecules connected through $NH\cdots O$ hydrogen bond between Ac protected substituents (coloured red)

forming $NH\cdots O$ hydrogen bonds. To quantify these interactions we decided to calculate interaction energies between pairs of molecules cut out from the crystal structure and optimized *in vacuo*, therefore without PCM formalism used in conformational analysis.

First, we have compared the single molecule geometries of **3b** (only heavy atoms) using experimental and both calculated structures (one optimized in $CHCl_3$ and one *in vacuo*). After the superposition the calculated root-mean-square deviations (RMSD) were 0.35 Å and 0.33 Å, respectively. Obviously, there was no significant distortion of geometry upon optimization *in vacuo* and in $CHCl_3$ modelled as polarizable continuum.

Second, we have compared each pair of molecules connected by intermolecular hydrogen bonds between substituents. As mentioned above, the unsymmetrically substituted **3b** has two distinctive molecular pairs depending whether hydrogen bond occurred between Ac or Boc protected substituents of each molecule (Fig. 14b and 14c). After optimization and comparison with crystal structure, the

obtained RMSD values were 1.29 Å and 0.99 Å, respectively. The calculated interaction energies corrected by basis set superposition error (BSSE) suggest a favourable interaction between two molecules of each chosen molecular pair. The values were -58.9 kJ mol^{-1} and -62.1 kJ mol^{-1} (corrected by basis set superposition error, BSSE), respectively. Without BSSE correction the obtained values were -66.3 kJ mol^{-1} and -72.1 kJ mol^{-1} . For comparison, the calculated interaction energy for two symmetrically substituted **3a** molecules was -62.9 kJ mol^{-1} (with BSSE) and -73.9 kJ mol^{-1} (without BSSE). This could also be a good indication of similar packing of molecules in symmetrically substituted **3c** for which, a single crystal, unfortunately, was not obtained.

Third, reorganization terms were also calculated as differences between the energies of each molecule based on geometry adopted in the optimized dimer and geometry of the most stable conformer. The corresponding values were less than 2 kJ mol^{-1} , thus requiring very small reorganization of single molecule geometry during crystal packing.

Fourth, the strength of interaction between pair of molecules in crystal structure of **3b** was compared with the similar interaction between two peptide strands in one molecule. Interaction energy between strands (engaging two hydrogen bonds) was estimated as the energy difference of two optimized geometries, the “open” conformer obtained from **3b-1** by adjusting the pseudo-torsion angle to approximately 180° , in which two substituents were not able to interact, and the most stable conformer **3b-1**, both optimized *in vacuo*. Considering all the approximations made in this approach, the calculated interaction energy amounts to -86 kJ mol^{-1} (not corrected by BSSE), *i.e.* for about 15 percent more than the interaction energy calculated between pair of **3b** molecules.

By taking into account all of these observations, one might conclude that derivatives **3** are capable to preserve the same IHB pattern consisted of two 10-membered β -turns in solution as well as in the solid state, thus making them a promising, yet simple scaffolds capable to mimic antiparallel β -sheet peptides.

Biological evaluation of bioconjugates **2a**, **3b** and **3c**

The ferrocene conjugates **3b** and **3c** synthesised in this work and previously reported Ac-Ala-Fca-Ala-OMe (**2a**)^{10c} were screened *in vitro* for their potential anticancer activity in Hep G2 human liver carcinoma cells and Hs 578T human breast cancer cells. [Since the comparable conformational pattern based on two simultaneous IHBs was seen in solution and in the solid state of analogue **2a**, we decided to test its biological activity as well].

The MTT assay, as an example of a widely applicable colorimetric endpoint assay, enables the indirect measurement of cytotoxicity as it involves the evaluation of mitochondrial dehydrogenase activity within the treatment period. In this method, the reduction of water-soluble tetrazolium salt MTT by metabolically active eukaryotic cells leads to precipitation of the colored formazans. It is assumed that dye reduction will be proportional to the number of viable cells in the exponential growth phase. Herein, the cells were treated with ferrocene and ferrocene conjugates **2a**, **3b** and **3c** at a range of concentrations 50 – 500 μM and cell viability was determined after 72 h. The summarized results of cytotoxicity evaluation in Hep G2 and Hs 578T cancer cell lines with a MTT bioassay are presented in Fig. 15. The IC_{50} values, presented in Table 4, were derived from the equations of related polynomial trend lines for each ferrocene conjugate.

The most of the metallodrugs currently tested and used in cancer treatment are based on platinum, in spite of negative medical and physical side-effects. For cisplatin, these include poor aqueous solubility, a high excretion rate from the body, loss of appetite (anorexia), development of drug resistance after continued drug dosage, high toxicity especially to the kidneys and bone marrow, and the most inconvenient, inability to distinguish between healthy and carcinoma cells.⁵⁷ Therefore, many efforts are focused on the investigation of the novel metal-based therapeutics, *i.e.* ferrocene conjugates with similar antineoplastic activity and fewer side effects as an alternative for platinum complex.

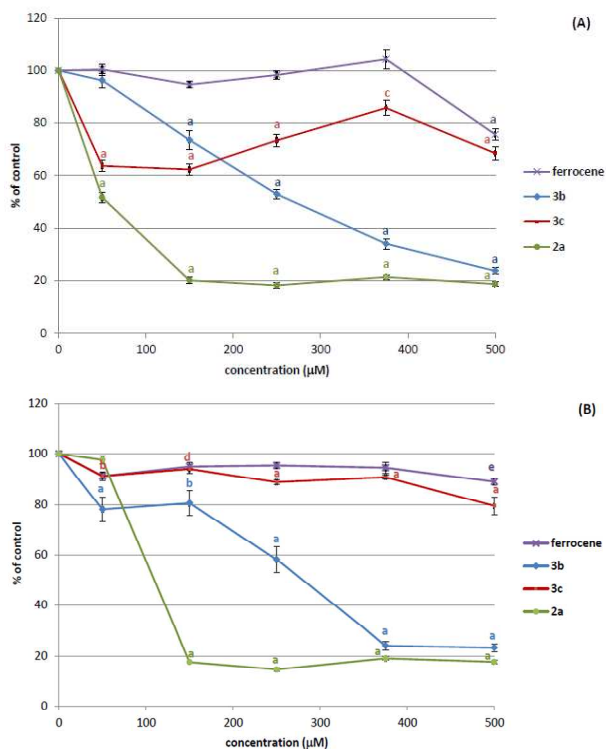


Figure 15. *In vitro* anti-proliferative effect of ferrocene and ferrocene conjugates **2a**, **3b** and **3c** against Hep G2 human liver carcinoma cells (A) and Hs 578T human breast cancer cells (B) obtained with MTT assay after 72 h exposure. Data are presented as percentage of control: mean \pm SEM of 3 experiments with 4 measurements within each experiment for each concentration. Statistical significance vs. control: ^a $p < 0.001$; ^b $p < 0.005$; ^c $p < 0.01$; ^d $p < 0.025$; ^e $p < 0.05$.

Table 4. IC_{50} values (μM) for ferrocene and ferrocene conjugates **2a**, **3b** and **3c** vs. Hep G2 human liver carcinoma cells and Hs 578T human breast cancer cells revealed by MTT cytotoxicity assay.

Compound	IC_{50} (μM)	
	Hs 578T	Hep G2
Ferrocene	[n.d.]	[n.d.]
3b	280.77	259.33
3c	[n.d.]	[n.d.]
2a	116.49	89.87

[n.d.] – non determined IC value for the corresponding incubation period, out of applied concentration range.

Ferrocene-acridine conjugates are pronounced among numerous ferrocene derivatives tested for antiproliferative purposes due to their highly cytotoxic activity.⁵⁸ The most significant anticancer applications of ferrocene derivatives is referred to hydroxyferrocifens, obtained by the replacement of one phenyl ring of the active metabolite tamoxifen with ferrocene moiety.⁵⁹

The presented data (Fig. 15, Table 4) reveal a cytotoxic potential of ferrocene conjugates **2a**, **3b** and **3c** against both cell lines. Ferrocene by itself had no significant effect on cell proliferation in concentrations up to 500 μM . However, a statistically significant reduction of the number of viable cells after treatment with 500 μM ferrocene ($p < 0.001$ for Hep G2

cells, $p < 0.05$ for Hs 578T) was observed. Ferrocene conjugates **2a**, **3b** and **3c** in concentrations of 150-500 μM significantly decreased cell proliferation ($p < 0.001 - p < 0.025$) (Fig. 15) and the highest cytotoxicity is obtained by compound **2a** in Hep G2 cells as well as in Hs 578T cells with slightly higher IC_{50} value (Table 4). For compound **3c**, IC_{50} data were out of applied concentration range indicating low activity (Table 4). Liver carcinoma cells Hep G2 were generally more sensitive to the tested compounds, but the trend of cytotoxicity was the same in the both cell lines - from the weakest effect provoked by compound **3c** to the most pronounced cell viability inhibition with compound **2a**.

The obtained IC_{50} values for herein studied ferrocene-containing peptides **2a**, **3b** and **3c** are still above IC_{50} for doxorubicin and cisplatin (literature data: 0.1 - 15 μM ; e.g. for cisplatin in Hep G2 cells $4.7 \pm 0.4 \mu\text{M}$) determined in different human cancer cell lines.^{39,60,61} Nevertheless, compound **2a** compared to other possess the most prominent cytotoxic activity against human breast and liver cancer cells. Hence, the conformational space of the tested peptides, based on two simultaneous interchain hydrogen bonds [$\text{NH}_{\text{Fn}} \cdots \text{OC}_{\text{Boc/Ac}}$ (**3b**, **3c**) as well as $\text{NH}_{\text{Fn}} \cdots \text{OC}_{\text{COOMe}}$ and $\text{NH}_{\text{Ala}} \cdots \text{OC}_{\text{Ac}}$ (**2a**)], is not of decisive influence on their biological activity. Our previous work on ferrocene peptides revealed the contribution of lipophilicity to biological activity.³⁹ Thus, the improved bioactivity of the bioorganometallics **2a** and **3b** is likely to be due to their increased lipophilicity (**2a**, $R_f = 0.24$; **3b**, $R_f = 0.51$) in comparison to the more polar peptide **3c** ($R_f = 0.12$). Therefore, the synthesis of similar compounds with profound biological activity is planned in our future work.

Conclusions

The employed synthetic route paves the way to bioorganometallics **3** containing ferrocene-1,1'-diamine substituted with peptide sequences of different structure and chirality that are expected to form intra- and intermolecular hydrogen bonds. A synthesis of orthogonally protected homochiral product Ac-Ala-NH-Fn-NH-Ala-Boc (**3b**) is reported for the first time. The detailed conformational analysis performed on novel compounds Ac-Ala-NH-Fn-NH-Ala-Boc (**3b**) and Fn-(NH-Ala-Ac)₂ (**3c**) shows a great preference for the formation of 14-membered rings (also labelled as two simultaneous 10-membered β -turns) between two substituents, no matter of Boc and/or Ac protection groups. The same pattern persists in solution, as well as in the solid state where it is accompanied by favorable intermolecular hydrogen bonds in the formation of infinite zig-zag chains.

Derivatives Ac-Ala-NH-Fn-NH-Ala-Boc (**3b**), Fn-(NH-Ala-Ac)₂ (**3c**) and Ac-Ala-Fca-Ala-OMe (**2a**) decreased cell proliferation in Hep G2 and Hs 578T cancer cell lines showing a cytotoxic ability in concentrations of 150-500 μM .

Whether this observations can be generalized to include other ferrocene-1,1'-diamine based derivatives remains to be seen. However, these results encourage us to extend our research on synthesis of more complex systems. Together with

the combination of spectroscopy, crystallography and computational analysis extended with biological evaluation tests it clearly establishes a protocol for extracting the valuable information about systems capable to mimic antiparallel β -sheet peptides.

With regard to the previously reported scaffolds Fcd and Fca, the herein employed ferrocene-1,1'-diamine (Fcd), as a constituent of yet still unexplored group of peptidomimetics **3**, shows a high potential to be considered as a stable and synthetically easily modifiable scaffold capable to preserve β -turns in solution as well as in the solid state, thus replicating hydrogen bonding pattern of peptide β -sheets.

Acknowledgements

This research was supported by the Ministry of Science, Education and Sports of the Republic of Croatia (Grant Numbers 058-1191344-3122, 119-1193079-3069 and 0582184-2232), Croatian Science Foundation under the project 7444 and University of Zagreb (PP1.30). Computational resources were provided by the Croatian National Grid Infrastructure (www.cro-ngi.hr) at Zagreb University Computing Centre (SRCE).

Notes and references

- 1 G. D. Rose, L. M. Gierasch and J. A. Smith, *Adv. Protein Chem.*, 1985, **37**, 1-109.
- 2 A. M. C. Marcelino and L. M. Gierasch, *Biopolymers*, 2008, **89**, 380-391.
- 3 B. Eckhardt, W. Grosse, L.-O. Essen and A. Geyer, *PNAS*, 2010, **107**, 18336-18341.
- 4 (a) B. Odaert, F. Jean, C. Boutillon, E. Buisine, O. Melnyk, A. Tartar and G. Lippens, *Protein Sci.*, 1999, **8**, 2773-2783.; (b) A. A. Fuller, D. Du, F. Liu, J. E. Davoren, G. Bhabha, G. Kroon, D. A. Case, H. J. Dyson, E. T. Powers, P. Wipf, M. Gruebele and J. W. Kelly, *PNAS*, 2009, **106**, 11067-11072.
- 5 D. J. Selkoe, *Nature*, 2003, **426**, 900-904.
- 6 (a) P. Chitnumsub, W. R. Fiori, H. A. Lashuel, H. Diaz and J. W. Kelly, *Bioorgan. Med. Chem.*, 1999, **7**, 39-59.; (b) J. S. Nowick, E. M. Smith, J. W. Ziller and A. J. Shaka, *Tetrahedron*, 2002, **58**, 727-739.; (c) O. Khakshoor and J. S. Nowick, *Curr. Opin. Chem. Biol.*, 2008, **12**, 722-729.; (d) J. S. Nowick, *Acc. Chem. Res.*, 2008, **41**, 1319-1330.; (e) P.-N. Cheng, J. D. Pham and J. S. Nowick, *J. Am. Chem. Soc.*, 2013, **135**, 5477-5492.
- 7 R. V. Nair, S. B. Baravkar, T. S. Ingole and G. J. Sanjayan, *Chem. Commun.*, 2014, **50**, 13874-13884.
- 8 (a) S. Chowdhury, G. Schatte and H.-B. Kraatz, *Angew. Chem. Int. Ed.*, 2008, **47**, 7056-7059.; (b) A. Lataifeh, S. Beheshti and H.-B. Kraatz, *Eur. J. Inorg. Chem.*, 2009, 3205-3218.; (c) T. Moriuchi and T. Hirao, *J. Inc. Phenom. Macrocycl. Chem.*, 2012, **74**, 23-40.
- 9 (a) A. Nomoto, T. Moriuchi, S. Yamazaki, A. Ogawa and T. Hirao, *Chem. Commun.*, 1998, 1963-1964.; (b) T. Moriuchi, A. Nomoto, K. Yoshida, A. Ogawa and T. Hirao, *J. Am. Chem. Soc.*, 2001, **123**, 68-75.; (c) T. Moriuchi, T. Nagai, T. Hirao, *Org. Lett.*, 2005, **7**, 5265-5268.; (d) T. Moriuchi, T. Nagai and T. Hirao, *Org. Lett.*, 2006, **8**, 31-34.; (e) T. Moriuchi, A. Nomoto, K. Yoshida and T. Hirao, *J. Organomet. Chem.*, 1999, **589**, 50-58.; (f) T. Moriuchi, A.

- Nomoto, K. Yoshida and T. Hirao, *Organometallics*, 2001, **20**, 1008-1013.; (g) T. Moriuchi and T. Hirao, *Acc. Chem. Res.*, 2010, **43**, 1040-1051.
- 10 (a) L. Barišić, M. Drodučić, V. Rapić, H. Pritzkow, S. I. Kirin and N. Metzler-Nolte, *Chem. Commun.*, 2004, 2004-2005.; (b) L. Barišić, M. Čakić, K. A. Mahmoud, Y.-n. Liu, H.-B. Kraatz, H. Pritzkow, S. I. Kirin, N. Metzler-Nolte and V. Rapić, *Chem. Eur. J.*, 2006, **12**, 4965-4980.; (c) L. Barišić, V. Rapić and N. Metzler-Nolte, *Eur. J. Inorg. Chem.*, 2006, 4019-4021.; (d) J. Lapić, D. Siebler, K. Heinze and V. Rapić, *Eur. J. Inorg. Chem.*, 2007, **14**, 2014-2024.; (e) M. Čakić Semenčić, D. Siebler, K. Heinze and V. Rapić, *Organometallics*, 2009, **28**, 2028-2037.; (f) M. Čakić Semenčić, K. Heinze, C. Förster and V. Rapić, *Eur. J. Inorg. Chem.*, 2010, 1089-1097.
- 11 S. Chowdhury, K. A. Mahmoud, G. Schatte and H.-B. Kraatz, *Org. Biomol. Chem.*, 2005, **3**, 3018-3023.
- 12 M. G. Bomar, B. Song, P. Kibler, K. Kodukula and A. K. Galande, *Org. Lett.*, 2011, **13**, 5878-5881.
- 13 L. Barišić, M. Kovačević, M. Mamić, I. Kodrin, Z. Mihalić and V. Rapić, *Eur. J. Inorg. Chem.*, 2012, **11**, 1810-1822.
- 14 Oxford Diffraction, Xcalibur CCD System. *CrysAlisPro*; Oxford Diffraction Ltd: Abingdon, England, 2013.
- 15 M. C. Burla, R. Caliendo, M. Camalli, B. Carrozzini, G. L. Casciarano, L. De Caro, C. Giacovazzo, G. Polidori and R. Spagna, *J. Appl. Crystallogr.*, 2005, **38**, 381-388.
- 16 G. M. Sheldrick, *Acta Crystallogr.*, 2008, **A64**, 112-122.
- 17 L. J. Farrugia, *J. Appl. Crystallogr.*, 2012, **45**, 849-854.
- 18 A. L. Spek, *Acta Crystallogr.*, 2009, **D65**, 148-155.
- 19 Maestro, version 9.7, Schrödinger, LLC, New York, NY, 2014.
- 20 MacroModel, version 10.3, Schrödinger, LLC, New York, NY, 2014.
- 21 F. Mohamadi, N. G. J. Richards, W. C. Guida, R. Liskamp, M. Lipton, C. Caufield, G. Chang, T. Henrickson, W. C. Still, *J. Comput. Chem.*, 1990, **11**, 440-467.
- 22 J. L. Banks, H. S. Beard, Y. Cao, A. E. Cho, W. Damm, R. Farid, A. K. Felts, T. A. Halgren, D. T. Mainz, J. R. Maple, R. Murphy, D. M. Philipp, M. P. Repasky, L. Y. Zhang, B. J. Berne, R. A. Friesner, E. Gallicchio, R. M. Levy, *J. Comp. Chem.*, 2005, **26**, 1752-1780.
- 23 Gaussian 09, Revision D.01, M. J. Frisch, G. W. Trucks, H. B. Schlegel, G. E. Scuseria, M. A. Robb, J. R. Cheeseman, G. Scalmani, V. Barone, B. Mennucci, G. A. Petersson, H. Nakatsuji, M. Caricato, X. Li, H. P. Hratchian, A. F. Izmaylov, J. Bloino, G. Zheng, J. L. Sonnenberg, M. Hada, M. Ehara, K. Toyota, R. Fukuda, J. Hasegawa, M. Ishida, T. Nakajima, Y. Honda, O. Kitao, H. Nakai, T. Vreven, J. A. Jr. Montgomery, J. E. Peralta, F. Ogliaro, M. Bearpark, J. J. Heyd, E. Brothers, K. N. Kudin, V. N. Staroverov, R. Kobayashi, J. Normand, K. Raghavachari, A. Rendell, J. C. Burant, S. S. Iyengar, J. Tomasi, M. Cossi, N. Rega, N. J. Millam, M. Klene, J. E. Knox, J. B. Cross, V. Bakken, C. Adamo, J. Jaramillo, R. Gomperts, R. E. Stratmann, O. Yazyev, A. J. Austin, R. Cammi, C. Pomelli, J. W. Ochterski, R. L. Martin, K. Morokuma, V. G. Zakrzewski, G. A. Voth, P. Salvador, J. J. Dannenberg, S. Dapprich, A. D. Daniels, Ö. Farkas, J. B. Foresman, J. V. Ortiz, J. Cioslowski, D. J. Fox, Gaussian, Inc., Wallingford CT, 2009.
- 24 D. Becke, *J. Chem. Phys.*, 1993, **98**, 5648-5652.
- 25 C. Lee, W. Yang, R. G. Parr, *Phys. Rev. B*, 1998, **37**, 785-789.
- 26 S. Grimme, J. Antony, S. Ehrlich, H. Krieg, *J. Chem. Phys.*, 2010, **132**, 154104.
- 27 E. Cancès, B. Mennucci, J. Tomasi, *J. Chem. Phys.*, 1997, **107**, 3032-3041.
- 28 E. Cancès, B. Mennucci, *J. Math. Chem.*, 1998, **23**, 309-326.
- 29 ChemBio3D Ultra 2012 v13, PerkinElmer Inc.
- 30 GaussView 5.0, R. Dennington, T. Keith, J. Millam, *Semichem Inc.*, Shawnee Mission, KS, 2009.
- 31 F. Biegler-König, J. Schönbohm, D. J. Bayles, *J. Comp. Chem.*, 2001, **22**, 545-559.
- 32 F. Biegler-König, J. Schönbohm, *J. Comp. Chem.*, 2002, **23**, 1489-1494.
- 33 J. J. McKinnon, M. A. Spackman, A. S. Mitchell, *Acta Crystallogr. Sect. B: Struct. Sci.*, 2004, **60**, 627.
- 34 F. L. Hirshfeld, *Theor. Chim. Acta*, 1977, **44**, 129.
- 35 Crystal Explorer (Version 3.1), S. K. Wolff, D. J. Grimwood, J. J. McKinnon, M. J. Turner, D. Jayatilaka, M. A. Spackman, University of Western Australia, 2012.
- 36 R. I. Freshney, *Culture of Animal Cells – a Manual of Basic Technique*, 2005, 5. ed., John Wiley & Sons, Inc., Hoboken, New Jersey.
- 37 M. Kovačević, V. Rapić, I. Lukač, K. Molčanov, I. Kodrin and L. Barišić, *J. Mol. Struct.*, 2013, **1048**, 349-356.
- 38 S. Djaković, D. Siebler, M. Čakić Semenčić, K. Heinze and V. Rapić, *Organometallics*, 2008, **27**, 1447-1453.
- 39 M. Kovačević, K. Molčanov, K. Radošević, V. Gaurina Srček, S. Roca, A. Čače and L. Barišić, *Molecules*, 2014, **19**, 12852-12880.
- 40 (a) S. Ganesh and R. Jayakumar, *Peptide Res.*, 2003, **59**, 249-256.; (b) V. S. Ananthanarayanan and T. S. Cameron, *Int. J. Peptide Protein Res.*, 1988, **31**, 399-411.; (c) L. Ning, W. De-Ning and Y. Sheng-Kang, *Polymer* 1996, **37**, 3045-3047.
- 41 D. Lehnerr, R. R. Tykewinski, *Org. Lett.*, 2007, **9**, 4583-4586.
- 42 (a) S. H. Gellman, G. P. Dado, G.-B. Liang and B. R. Adams, *J. Am. Chem. Soc.*, 1991, **113**, 1164-1173.; (b) A. Pardi, G. Wagner and K. Wuthrich, *Eur. J. Biochem.*, 1983, **137**, 445-454.
- 43 (a) M. Llinás and M. P. Klein, *J. Am. Chem. Soc.*, 1975, **97**, 4731-4737.; (b) H. Kessler, *Angew. Chem.*, 1982, **94**, 509-520; *Angew. Chem. Int. Ed. Engl.*, 1982, **21**, 512-523.; (c) M. Iqbal and P. Balaram, *Biopolymers*, 1982, **21**, 1427-1433.; (d) E. K. S. Vijayakumar and P. Balaram, *Biopolymers*, 1983, **22**, 2133-2140.; (e) N. H. Andersen, J. W. Neidigh, S. M. Harris, G. M. Lee, Z. Liu and H. Tong, *J. Am. Chem. Soc.*, 1997, **119**, 8547-8561.; (f) N. J. Baxter and M. P. Williamson, *J. Biomol. NMR*, 1997, **9**, 359-369.; (g) H.-J. Lee, H.-M. Park and K. B. Lee, *Biophys. Chem.*, 2007, **125**, 117-126.; (h) T. Cierpicki, I. Zhukov, R. A. Byrd and J. Otlewski, *J. Magn. Reson.*, 2002, **157**, 178-180.
- 44 (a) F. E. Appoh, T. C. Sutherland and H.-B. Kraatz, *J. Organomet. Chem.*, 2004, **689**, 4669-4677.; (b) J. Lapić, G. Pavlović, D. Siebler, K. Heinze and V. Rapić, *Organometallics*, 2008, **27**, 726-735.
- 45 E. S. Stevens, N. Sugawara, G. M. Bonora and C. Toniolo, *J. Am. Chem. Soc.*, 1980, **102**, 7048-7050.
- 46 (a) K. A. Dill, *Biochemistry US*, 1990, **29**, 7133-7155.; (b) A. W. Fitzpatrick, T. P. J. Knowles, C. A. Waudby, M. Vendruscolo, C. M. Dobson, *PLoS Comp. Biol.*, 2011, **7**, e1002169.
- 47 (a) T. P. Curran, K. A. Marques, M. V. Silva, *Org. Biomol. Chem.*, 2005, **3**, 4134-4138.; (b) S. Hanessian, G. Papeo, K. Fettes, E. Therrien and M. T. P. Viet, *J. Org. Chem.*, 2004, **69**, 4891-4899.; (c) S. K. Maji, D. Haldar, D. Bhattacharyya and A. Bannerjee, *J. Mol. Struct.*, 2003, **646**, 111-123.; (d) S. Vijayalakshmi, R. B. Rao, I. L. Karle and P. Balaram, *Biopolymers*, 2000, **53**, 84-98.; (e) R. M. Jain, K. R. Rajashankar, S. Ramakumar and V. S. Chauhan, *J. Am. Chem. Soc.*, 1997, **119**, 3205-3211.; (f) R. S. Herrick, R. M. Jarret, T. P. Curran, D. R. Dragoli, M. B. Flaherty, S. E. Lindyberg, R. A. Slate and L. C. Thornton, *Tetrahedron Lett.*, 1996, **37**, 5289-5292.; (g) A. Mollica, M. Paglialunga

- Paradisi, D. Torino, S. Spisani and G. Lucente, *Amino Acids*, 2006, **30**, 453-459.; (h) F. Sladojevich, A. Guarna and A. Trabocchi, *Org. Biomol. Chem.*, 2010, **7**, 916-924.
- 48 V. Kovač, M. Čakić Semenčić, I. Kodrin, S. Roca and V. Rapić, *Tetrahedron*, 2013, **69**, 10497-10506.
- 49 (a) D. B. Dahl, Z. Bohannan, Q. Mo, M. Vannucci and J. Tsai, *J. Mol. Biol.*, 2008, **378**, 749-758.; (b) A. Q. Zhou, D. Caballero, C. S. O'Hern and L. Regan, *Biophys. J.*, 2013, **105**, 2403-2411.
- 50 J. S. Nowick and S. Insaf, *J. Am. Chem. Soc.*, 1997, **119**, 10903-10908.
- 51 J. Bernstein, R. E. Davis, L. Shimoni, N-L. Chang, *Angew. Chem. Int. Ed. Engl.*, 1995, **34**, 1555-1573.
- 52 J. Lapić, S. Djaković, M. Cetina, K. Heinze and V. Rapić, *Eur. J. Inorg. Chem.*, 2010, 106-114.
- 53 S. R. Batten and R. Robson, *Angew. Chem. Int. Ed. Engl.*, 1998, **37**, 1460-1494.
- 54 (a) J. Lapić, S. Djaković, I. Kodrin, Z. Mihalić, M. Cetina, V. Rapić, *Eur. J. Org. Chem.*, 2010, **13**, 2512-2524.; (b) S. Djaković, I. Kodrin, V. Smrečki, P. Novak, Z. Mihalić, D. Žihor, J. Lapić, V. Rapić, *Tetrahedron*, 2014, **70**, 2330-2342.; (c) M. Čakić-Semenčić, V. Kovač, I. Kodrin, L. Barišić, V. Rapić, *Eur. J. Inorg. Chem.*, 2015, 112-123
- 55 U. Koch, P. L. A. Popelier, *Phys. Chem.*, 1995, **99**, 9747.
- 56 P. L. A. Popelier, *J. Phys. Chem. A*, 1998, **102**, 1873.
- 57 J. C. Swarts, S. J. Vosoloo, S. J. Cronje, W. C. Du Plessis, C. E. Van Rensburg, E. Kreft, J. E. Van Lier, *Anticancer Res.*, 2008, **28**, 2781-2784.
- 58 G. Gasser, I. Ott, N. Metzler-Nolte, *J. Med. Chem.*, 2011, **54**, 3-25.
- 59 G. Jaouen, S. Top, A. Vessières, G. Leclercq, M. J. McGlinchey, *Curr. Med. Chem.*, 2004, **11**, 2505-2017.
- 60 J. A. McAlpine, H. T. Lu, K. C. Wu, S. K. Knowles, J. A. Thomson, *BMC Cancer*, 2014, **14**, 621- 633.
- 61 R. Cortés, M. Crespo, L. Davin, R. Martín, J. Quirante, D. Ruiz, R. Messeguer, C. Calvis, L. Baldomà, J. Badia, *Eur. J. Med. Chem.*, 2012, **54**, 557-566.